


Exact ground states and phase diagram of the quantum compass model under an in-plane field

A. D. S. Richards* and Erik S. Sørensen[†]

Department of Physics and Astronomy, McMaster University, Hamilton, Ontario, Canada, L8S 4M1

 (Received 3 October 2023; revised 13 June 2024; accepted 17 June 2024; published 26 June 2024)

We consider the square lattice $S = 1/2$ quantum compass model (QCM) parametrized by J_x, J_z , under a field, \mathbf{h} , in the x - z plane. At the special field value $(h_x^*, h_z^*) = 2S(J_x, J_z)$, we show that the QCM Hamiltonian may be written in a form such that two simple product states can be identified as exact ground states, below a gap. Exact excited states can also be found. We use the staggered vector chirality to characterize the exact ground states at (h_x^*, h_z^*) and states obtained for fields within the vicinity of (h_x^*, h_z^*) . This gapped phase occupies most of the in-plane field phase diagram. For some values of $h_x > h_z$ and $h_z > h_x$ at the edges of the phase diagram, we have found transitions between this gapped phase and phases of weakly coupled Ising-chain states. In zero field, the QCM is known to have an emergent subextensive ground-state degeneracy. As the field is increased from zero, we find that this degeneracy is partially lifted, resulting in bond-oriented spin-stripe states, which are each separated from one another and the gapped phase by first-order transitions. Our findings are important for understanding the field dependent phase diagram of materials with predominantly directionally dependent Ising interactions.

DOI: [10.1103/PhysRevB.109.L241116](https://doi.org/10.1103/PhysRevB.109.L241116)

Quantum compass models were first introduced as a model of orbital-orbital interactions arising from a Jahn-Teller distortion [1–4], and both classical and quantum versions have been extensively studied [5–19] with the main focus on ground-state properties of two-dimensional models. Interest in compass models intensified with the realization that Kitaev’s honeycomb model [20] with bond-directional interactions, a special case of a compass model, potentially can be realized in materials through a superexchange mechanism [21]. In particular, iridium- and ruthenium-based systems in which ligands form edge-sharing octahedra surrounding the transition metal atoms have been proposed as materials which may realize a pseudospin Kitaev model [21], with α -RuCl₃ [22–24], a layered two-dimensional honeycomb material, as one of the most promising materials. This has given rise to the class of Kitaev materials [25–30] that one may view as particular realizations of the broader class of quantum compass models. For Kitaev materials, field-induced spin liquid phases are of special interest due to the potential presence of anyonic excitations, and intriguing results have been observed in theoretical studies [31–45] and in recent experiments on α -RuCl₃ when an out-of-plane field [46] is applied in the [111] direction, as well as for an in-plane field [47–51]. The latter case is of special interest here since we show that for the closely related square lattice quantum compass model (QCM) a twice degenerate exact ground-state below a gap can be found under an in-plane field, inducing an extended phase with other nontrivial phases in proximity. Here, we determine the complete in-plane field phase diagram.

The bulk of our results are focused on the QCM, and we first note a number of interesting properties of this model. The QCM on a lattice of linear size L , in the absence of a magnetic field, has a subextensive ground-state degeneracy of 2×2^L [9] and topological soliton excitations which are deconfined in one dimension [52]. Through a duality transformation [8], it has been shown that the QCM is equivalent to the Xu-Moore model, originally proposed to model interactions between $p + ip$ superconductor arrays [53]. Furthermore, a duality mapping has also been established between the Xu-Moore model and the transverse-field toric code model [54,55]. Consequently, a duality mapping exists between the zero field QCM and the transverse field toric code model, and the latter model has been studied under an in-plane field [56] as well as a transverse field [55]. Both classical and quantum QCM models have been studied at finite temperature [7,11], in both cases finding a transition in the two-dimensional (2D) Ising universality class to a low temperature ordered phase. One may also note that, it has been shown in Ref. [57] that two decoupled copies of the QCM can be mapped to the model of interacting Majorana fermions of Ref. [57], relevant to 3D topological insulators with proximity-induced superconductivity. Dualities between each of these models demonstrate how properties of the QCM may be understood in several different contexts. Finally, materials that likely realize the QCM have been identified in the strong spin-orbit coupled iridates, such as Ba₂IrO₄ [58] and Tb-substituted Sr₂IrO₄ [59,60]. The antiferromagnetic quantum compass model is

$$\mathcal{H} = J \sum_{\mathbf{r}} (\hat{S}_{\mathbf{r}}^x \hat{S}_{\mathbf{r}+e_x}^x + \hat{S}_{\mathbf{r}}^z \hat{S}_{\mathbf{r}+e_z}^z) - \sum_{\mathbf{r}} \mathbf{h} \cdot \hat{\mathbf{S}}_{\mathbf{r}}. \quad (1)$$

Here, we set $g = \hbar = \mu_B = 1$. Furthermore, we parametrize the field term as $\mathbf{h} = h(\cos \phi_{xz}, 0, \sin \phi_{xz})$ and define $|\mathbf{h}| = h$

*Contact author: richaa12@mcmaster.ca

[†]Contact author: sorensen@mcmaster.ca

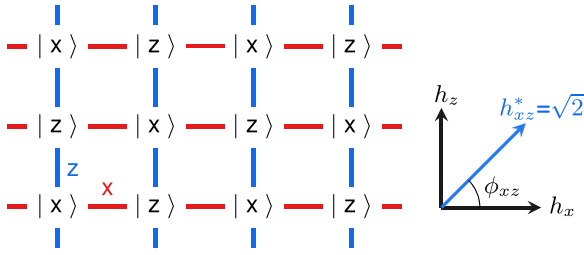


FIG. 1. Exact ground state of the QCM under in-plane field $h_{xz}^* = 2JS\sqrt{2}$. Colored bonds represent Ising interactions.

as the field strength. We use $N = L_x \times L_z$ to denote the number of sites in the model, and we shall refer to the $J\hat{S}^x\hat{S}^x$ coupling as a x bond and the $J\hat{S}^z\hat{S}^z$ coupling as a z bond. In zero field, a unitary transformation around the y axis on every second site relates J to $-J$. However, since our focus is on ground states in the presence of a field, the sign of J matters, and we exclusively focus on the antiferromagnetic (AF) model with $J > 0$. We set $J = 1$.

Exact ground and excited states. The exact ground states for the QCM can be found by the following simple argument. If we consider the Hamiltonian, Eq. (1) for general S , we can write the field term in the form $-\sum_{\mathbf{r}}(h_x\hat{S}_{\mathbf{r}}^x + h_z\hat{S}_{\mathbf{r}}^z)$. Following Refs. [61,62], we then see that with $\phi_{xz} = \pi/4$, where $h_x = h_z$, we can absorb the field term into the interaction term at the special field value $h_x^* = h_z^* = 2JS$ with $|h_{xz}^*| = 2JS\sqrt{2}$. For an $L_x \times L_z$ lattice with periodic boundary conditions in both directions and both L_x and L_z even, we can then write at h_{xz}^*

$$\mathcal{H} = \mathcal{H}_p - 2NJS^2$$

$$\mathcal{H}_p = J \sum_{\mathbf{r}} [(S - \hat{S}_{\mathbf{r}}^x)(S - \hat{S}_{\mathbf{r}+e_x}^x) + (S - \hat{S}_{\mathbf{r}}^z)(S - \hat{S}_{\mathbf{r}+e_z}^z)]. \quad (2)$$

\mathcal{H}_p is here positive semidefinite, and it follows that if a product state $|P\rangle$ can be found where each site is in an eigenstate of $\hat{S}^\alpha|\alpha\rangle = S|\alpha\rangle$ ($\alpha = x, z$) such that $\mathcal{H}_p|P\rangle = 0$, then $|P\rangle$ is not only an eigenstate, but a ground state. For the QCM it is straightforward to see that if L_x and L_z are both even, and periodic boundary conditions (PBC) are applied, then the two simple product states with $|x\rangle$ on one sublattice and $|z\rangle$ on the other, as shown in Fig. 1, are eigenstates of \mathcal{H}_p with eigenvalue 0, and therefore degenerate ground states with $E_0 = -2NJS^2$. This construction trivially generalizes to the case where $J_x \neq J_z$ where the same ground states appear at $(h_x^*, h_z^*) = 2S(J_x, J_z)$. It is exact for any finite $L_x \times L_z$ torus under PBC, but does not hold for open boundary conditions (OBC) nor when L_x or L_z are odd. It is interesting to note that the above argument is only superficially related to the remarkable extension of the Lieb-Schultz-Mattis (LSM) theorem for quantum spin chains [63,64] to the case of an applied field [65,66], showing that magnetization plateaus can appear, associated with a gapped state, when conserved quantities such as the total magnetization $\sum_j S_j^z$ are present. In contrast, for the QCM, the magnetization is not conserved, and since we can generalize to the case $J_x \neq J_z$, any special symmetry axis does not appear important. We also note that similar

product states formed with $S^\alpha|\alpha_m\rangle = m|\alpha_m\rangle$ with $0 < m < S$ will be eigenstates at the field value $h_x = h_z = 2Jm$, but not ground states. In the following, we provide strong numerical evidence for a sizable gap at h_{xz}^* and demonstrate that the two product states are the *only* ground states at h_{xz}^* under periodic boundary conditions (PBC) with L_x, L_z even. We expect that, for large systems, lifting these constraints will not change the physics due to the presence of a gap, and we explore the full phase diagram using infinite projected entangled pair states (iPEPS), without imposing PBC.

Methods. For an in-plane field there is no sign problem and Monte Carlo methods are applicable, but we have found it advantageous to use iPEPS [67–69] directly in the thermodynamic limit for the two-dimensional lattice, to obtain high precision results for the field dependent phase diagram of the QCM at zero temperature. For details, see the Supplemental Material [70]. In addition, we use exact diagonalization (ED) of small clusters, and infinite-size density matrix renormalization group (iDMRG) [71–78] on infinitely long cylinders in the x direction, of circumference up to $L_z = 10$. Typically, we use iDMRG with a bond dimension up to $D = 1000$ and $\epsilon = 10^{-11}$. The locations of quantum critical points (QCP) are first determined from the susceptibility of the ground state energy per spin e_0 with respect to a parameter p , defined as $\chi_p^e = -\frac{\partial^2 e_0}{\partial p^2}$. In finite systems, at a quantum critical point, χ^e is known to scale as [79–81] $\chi^e \sim N^{2/\nu-d-z}$, and is therefore likely to diverge at a QCP, with ν and z the correlation and dynamical critical exponents and d the spatial dimension.

For the remainder of our results, we specialize our calculations to the case of $S = 1/2$. In light of our exact solution mentioned previously, and the bond-directional ordering of the QCM in zero field, we define the vector bond chirality

$$\mathcal{X}_\alpha^y = \langle \vec{S}_{\mathbf{r}} \times \vec{S}_{\mathbf{r}+e_\alpha} \rangle^y, \quad \alpha = x, z \quad (3)$$

along with a nematic order parameter

$$\phi = \langle S_{\mathbf{r}}^x S_{\mathbf{r}+e_x}^x - S_{\mathbf{r}}^z S_{\mathbf{r}+e_z}^z \rangle. \quad (4)$$

quantifying the degree of orthogonality and bond-directional alignment of neighboring spins respectively. We have also found it useful to denote the vector chirality averaged over bond directions as $\mathcal{X}^y = \frac{1}{2}(\mathcal{X}_x^y + \mathcal{X}_z^y)$.

Phases under [101] field. Our iPEPS, iDMRG, and ED calculations can clearly distinguish two phase transitions when varying the strength of the in-plane field along the constant angle $\phi_{xy} = \frac{\pi}{4}$ as shown in Fig. 2. The high-field phase is a trivial polarized state (PS). Upon lowering the field, at the upper critical field $h_{xz}^{c2} = 1.626$, the PS transitions into a phase with substantial vector chirality (SVC). This can be seen in Fig. 2(b), where, at h_{xz}^{c2} , $|\mathcal{X}^y|$ increases, seemingly continuously, from zero in the PS, while a divergence in $|\chi_{h_{xz}}^e|$ is observed. Within the SVC phase, bond correlations of the form $\langle S^\alpha S^\alpha \rangle$, with $\alpha = (x, y, z)$, tend to zero as the state approaches the exactly solved states (shown in Fig. 1), at $h_{xz}^* = 2JS\sqrt{2}$. ED results for the gaps, in Fig. 2(c), show that the SVC phase is gapped with a twofold degenerate ground state. A second transition into a low-field region with stripe ordering, occurs as the field is lowered below $h_{xz}^{c1} = 0.540$.

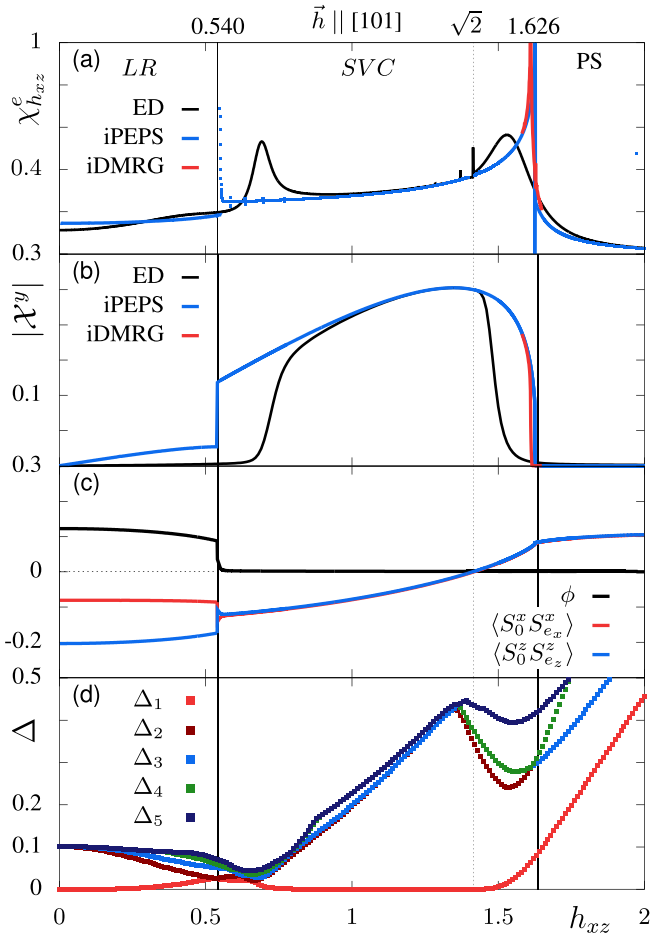


FIG. 2. Results from ED with PBC on a 4×6 lattice, iDMRG with $L_z = 10$, and iPEPS versus field strength, h_{xz} , for a field in the [101] direction ($\phi_{xz} = \pi/4$). (a) $\chi_{h_{xz}}^e$ ED, iPEPS, and iDMRG. (b) $|\mathcal{X}^y|$ from ED with a small pinning field $0.005h_z$ on a single site, iPEPS, and iDMRG. (c) ϕ and bond correlations from iPEPS. (d) First five lowest energy gaps, Δ_i , as obtained from ED. Solid vertical lines indicate $h_{xz}^{c1} = 0.540$ and $h_{xz}^{c2} = 1.626$ separating the low field L , R , SVC , and polarized (PS) states. The dotted vertical line indicates the exactly solvable point, $h_{xz}^* = 2SJ\sqrt{2}$.

Within the low field region, the line $h_x = h_z$ for $h_{xz} < h_{xz}^{c1}$ is a first-order critical line, terminating at h_{xz}^{c1} , separating phases of x -aligned and z -aligned stripe states [70] that we denote by L and R (see Fig. 4). As the field is lowered further to $h_{xz} = 0$, we find that the nematic order parameter, shown in Fig. 2(c), saturates to $\phi = 0.123$, in agreement with previous quantum Monte Carlo calculations [10,11].

Phases under [100] field. Notably, the zero-field QCM has the 1D gauge-like symmetries,

$$P_i = \prod_j S_{ie_x+je_z}^x \quad \text{and} \quad Q_i = \prod_j S_{je_x+ie_z}^z, \quad (5)$$

where the P_i and Q_i are incompatible. Arguments based on symmetry analysis imply that the $S = 1/2$ QCM ground state is at least twofold degenerate [82]. However, exact diagonalization calculations indicate that, when $L_x = L_z$, $2 \times 2^{L_x} - 2$ low-energy states collapse onto the twofold ground states

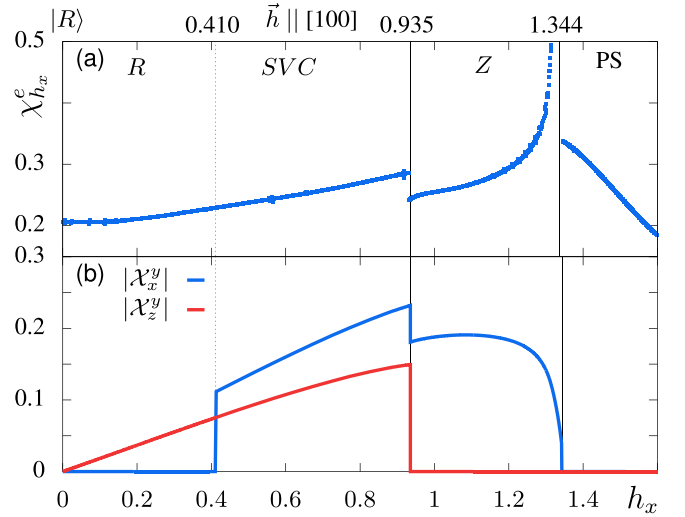


FIG. 3. (a) $\chi_{h_x}^e$ and (b) $|\mathcal{X}_x^y|$ and $|\mathcal{X}_z^y|$ as obtained from iPEPS calculations versus field strength, h_x , for a field parallel to [100] ($\phi_{xz} = 0$). Solid vertical lines indicate $h_x^{c1} = 0.935$ and $h_x^{c2} = 1.344$ separating the SVC , Z , and polarized (PS) states. A dashed line at $h_x = 0.410$ indicates the limiting value of the transition between R and SVC phases as $h_z \rightarrow 0$.

exponentially fast with increasing L_x [9], implying an emergent subextensive degeneracy in the thermodynamic limit. Following Ref. [12], we label the eigenstates of the P_i and Q_i as $|R\rangle$ and $|L\rangle$, respectively.

We have found that adiabatically evolving the $|R\rangle$ and $|L\rangle$ states under a small [100] field, h_x , produces an energy splitting between the two states, with the $|R\rangle$ -evolved state, $|R(\vec{h})\rangle$, having lower energy than the $|L\rangle$ -evolved state, $|L(\vec{h})\rangle$, for $h_x > h_z$. On the other hand, for a small [001] field, h_z , it is $|L(\vec{h})\rangle$ that has the lowest energy. Consequently, as outlined above, there is a first-order transition between the $|L(\vec{h})\rangle$ and $|R(\vec{h})\rangle$ states along the line $h_x = h_z$ [70], reminiscent of the first-order transition studied in Ref. [12]. We find that this line of first-order transitions terminates at the critical point, $h_{xz}^{c1} = 0.540$, discussed in the previous section. We may then view h_{xz}^{c1} as a multicritical point since the R , L , and SVC phases all meet at this point. Furthermore, our calculations indicate that, in zero field, the $|R\rangle$ and $|L\rangle$ states are sub-extensively degenerate, and that these degeneracies are lifted when small finite fields are applied [70].

With a field in the [100] direction, the high field PS again undergoes a transition as the field is lowered below a critical field $h_x^{c2} = 1.344$, as can be seen by the sharp divergence of $\chi_{h_x}^e$ in Fig. 3(a). However, in this case, the ground state consists approximately of alternating linear domains of field-polarized spins and antiferromagnetically ordered spins perpendicular to the field. The vector chirality is therefore nonzero when evaluated on bonds connected to polarized spins, as shown in Fig. 3(b), but only across bonds in the [100] direction. This phase has an interesting interpretation: columns of x -polarized spins lower the energy by aligning with the field, while columns of z -oriented spins form strongly coupled antiferromagnetic Ising chains. Due to the nature of the QCM coupling, the two kinds of columns are not coupled.

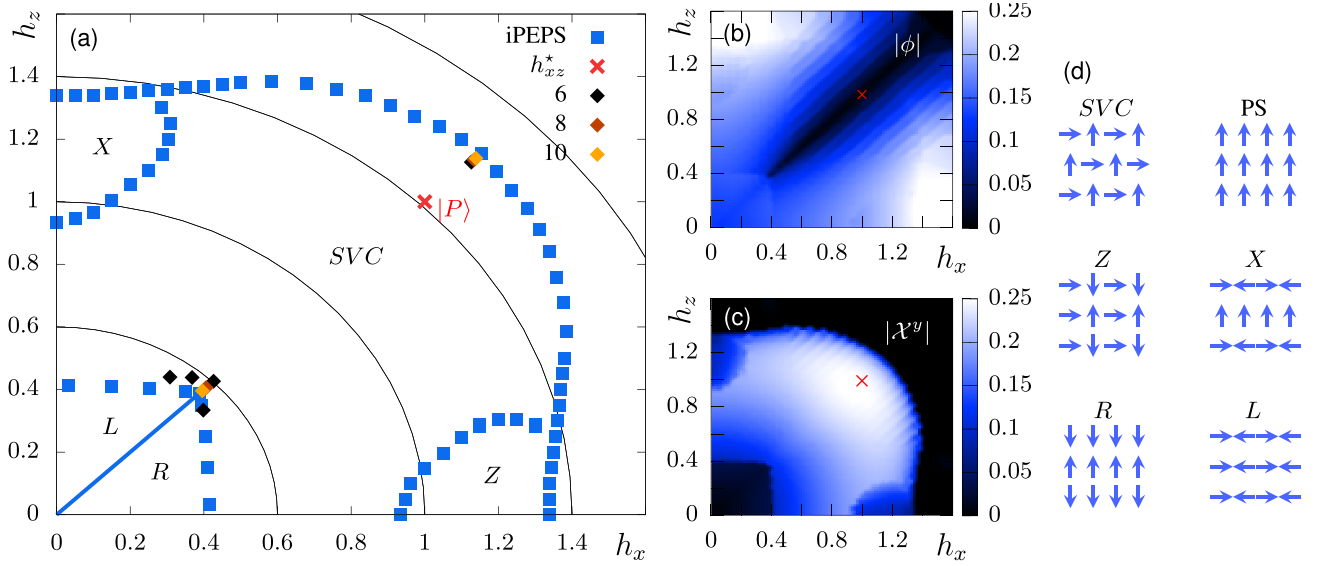


FIG. 4. (a) Phase diagram for the quantum compass model under an in-plane field. The phases are labeled as z -oriented stripe (R), x -oriented stripe (L), staggered vector chiral (SVC), z chain (Z), and x chain (X). We show iPEPS results (blue squares) and iDMRG (colored diamonds) for $L_z = 6, 8, 10$. Solid black lines are contours of constant field strength. (b) $|\phi|$ and (c) $|\mathcal{X}^y|$ as obtained from iPEPS for an in-plane field. (d) Dominant ordering of states in the labeled phases; the PS state is meant to show alignment in the field direction.

This suggests that this state is effectively one-dimensional in nature. For this reason, we refer to this phase as the z -chain (Z) phase, since the columns of spins polarized along x direction are essentially inert, although their presence effectively eliminates the coupling between the z chains. A sketch of the spin alignments in the Z phase is shown in Fig. 4. As the field is lowered further, a second transition from the Z phase to the SVC phase occurs at $h_x^{c1} = 0.935$. Finally, as $h_x \rightarrow 0$, the iPEPS approaches the $|R\rangle$ state. With $h_z = 0$, the transition from the SVC phase to the R phase is not directly visible in $\chi_{h_x}^e$, but the dashed line in Fig. 3 indicates the limiting value of the transition between R and SVC phases as $h_z \rightarrow 0$, at $h_x = 0.410$. By symmetry of the model, for a field along the z direction an analogous phase, X , appears along the z axis. The X phase is dominated by rows of spins coupled by antiferromagnetic x bonds.

Phase diagram. We have also analyzed the complete phase diagram for a range of field values, $h_x, h_z > 0$. The results of our calculations produce the phase diagram as shown in Fig. 4. The most apparent feature of the phase diagram is the large phase surrounding the point h_{xz}^* , where the product states $|P\rangle$, from Fig. 1 are exact ground states. As shown in panel (c) of Fig. 4, the vector chirality, $|\mathcal{X}^y|$, is found to be substantial throughout this phase, reduced in the Z and X phases, and approaching zero in the low field L, R regime. The nematic order parameter, ϕ , is close to zero in the intermediate-field regime for field angles near $\pi/4$ reflecting a lack of spin alignment along bond directions. In the low-field regime, bond alignment is found to dominate, with $|\mathcal{X}^y|$ taking a value near zero. Remarkably, we find that the transition between the R and SVC phases is almost independent of h_z . Likewise, we find the transition between the L and SVC phases to be independent of h_x . The combined R and L phases therefore form a square in the lower left part of the phase diagram, similar to what is seen for the toric code [56]. Even though the field is not applied along an easy axis it is natural to view

the SVC phase as a spin-flopped phase [83], and therefore to expect all transitions between the R, L, X , and Z to be first order. As it turns out, all our calculations are consistent with this [70]. However, from our calculations, the transition to the PS phase appears to be continuous.

Discussion. For the AF QCM we have shown that two exact ground states exist at the special field value $h_x^* = h_z^* = 2JS$. This special point has a substantial (staggered) vector chirality $|\mathcal{X}^y|$ and a sizable gap, inducing the SVC phase that dominates a large part of the phase diagram. Although our numerical results clearly indicate a sizable gap at h_{xz}^* within the SVC , establishing a rigorous proof of this gap would be of considerable interest. Our detailed study of the model under an in-plane magnetic field shows that, aside from the high field PS state, there are five distinct phases in the low to intermediate field regime, the SVC, Z, X, L , and R phases. Excitations in these phases could be nontrivial. For instance, in zero-field one-dimensional solitonic excitations [52] have been noted, and it is possible that they remain deconfined in the L and R phases, as has been observed for the toric code under an in-plane field [56] and the X-cube fracton model [84]. Perhaps the most surprising thing about the phase diagram is the existence of the SVC phase and accompanying transition to the PS phase since one might expect the system to transition from the low field L, R phases directly to the PS phase, without an intermediate phase. It is also important to consider similar exact product states in Kitaev's honeycomb model (KHCM) [20] with antiferromagnetic couplings, K_x, K_y, K_z . For the KHCM it is possible to again write the Hamiltonian in the same form as Eq. (2), in terms of a \mathcal{H}_p , at the field $(h_x^*, h_y^*, h_z^*) = S(K_x, K_y, K_z)$ (note the factor of 2 difference with respect to the QCM). Unfortunately, for the KHCM it is not geometrically possible to find an assignment of the $|x\rangle, |y\rangle$, and $|z\rangle$ states to the lattice which is an eigenstate of \mathcal{H}_p with eigenvalue 0, in the same way as it is done here for the QCM. Analogous exact product states therefore do not

exist for the KHCM. We also note that the KHCM, at the corresponding field value of $|h^*| = KS\sqrt{3}$ for the isotropic model, is known to be in the polarized phase for a field in the [111] direction and not in the candidate spin liquid phase [36,85]. The product states discussed here are therefore likely not pertinent for the KHCM. Despite this, it seems likely that similar phases can be found in other materials with predominantly directionally dependent Ising interactions, the crucial ingredient being a low coordination number lattice where a product eigenstate can be found. Our work motivates

further studies of materials-relevant Hamiltonians including the isotropic Heisenberg interaction [86], which is likely non-negligible in Ba_2IrO_4 [58] and Tb-substituted Sr_2IrO_4 [59,60].

Acknowledgments. We acknowledge the support of the Natural Sciences and Engineering Research Council of Canada (NSERC) through Discovery Grant No. RGPIN-2017-05759. We thank H.-Y. Kee for fruitful discussions. This research was enabled in part by support provided by SHARCNET [87] and the Digital Research Alliance of Canada [88].

-
- [1] K. I. Kugel' and D. I. Khomskii, Superexchange ordering of degenerate orbitals and magnetic structure of dielectrics with Jahn-Teller ions, *JETP Lett.* **15**, 446 (1972).
- [2] K. I. Kugel' and D. I. Khomskii, Crystal structure and magnetic properties of substances with orbital degeneracy, *Zh. Eksp. Teor. Fiz.* **64**, 429 (1973).
- [3] K. I. Kugel and D. Khomskii, The Jahn-Teller effect and magnetism: transition metal compounds, *Sov. Phys. Usp.* **25**, 231 (1982).
- [4] D. I. Khomskii, Review-orbital physics glorious past, bright future, *ECS J. Solid State Sci. Technol.* **11**, 054004 (2022).
- [5] M. Ferrero, F. Becca, and F. Mila, Freezing and large time scales induced by geometrical frustration, *Phys. Rev. B* **68**, 214431 (2003).
- [6] C. Ulrich, G. Khaliullin, J. Sirker, M. Reehuis, M. Ohl, S. Miyasaka, Y. Tokura, and B. Keimer, Magnetic neutron scattering study of YVO_3 : Evidence for an orbital Peierls state, *Phys. Rev. Lett.* **91**, 257202 (2003).
- [7] A. Mishra, M. Ma, F.-C. Zhang, S. Guertler, L.-H. Tang, and S. Wan, Directional ordering of fluctuations in a two-dimensional compass model, *Phys. Rev. Lett.* **93**, 207201 (2004).
- [8] Z. Nussinov and E. Fradkin, Discrete sliding symmetries, dualities, and self-dualities of quantum orbital compass models and $p + ip$ superconducting arrays, *Phys. Rev. B* **71**, 195120 (2005).
- [9] J. Dorier, F. Becca, and F. Mila, Quantum compass model on the square lattice, *Phys. Rev. B* **72**, 024448 (2005).
- [10] T. Tanaka and S. Ishihara, Dilution effects in two-dimensional quantum orbital systems, *Phys. Rev. Lett.* **98**, 256402 (2007).
- [11] S. Wenzel and W. Janke, Monte Carlo simulations of the directional-ordering transition in the two-dimensional classical and quantum compass model, *Phys. Rev. B* **78**, 064402 (2008).
- [12] R. Orús, A. C. Doherty, and G. Vidal, First order phase transition in the anisotropic quantum orbital compass model, *Phys. Rev. Lett.* **102**, 077203 (2009).
- [13] W.-L. You, G.-S. Tian, and H.-Q. Lin, The low-energy states and directional long-range order in the two-dimensional quantum compass model, *J. Phys. A: Math. Theor.* **43**, 275001 (2010).
- [14] F. Trouselet, A. M. Oleś, and P. Horsch, Compass-Heisenberg model on the square lattice—spin order and elementary excitations, *Europhys. Lett.* **91**, 40005 (2010).
- [15] W. Brzezicki and A. M. Oleś, Symmetry properties and spectra of the two-dimensional quantum compass model, *Phys. Rev. B* **87**, 214421 (2013).
- [16] H. T. Wang and S. Y. Cho, Long-range string orders and topological quantum phase transitions in the one-dimensional quantum compass model, *J. Phys.: Condens. Matter* **27**, 015603 (2015).
- [17] Z. Nussinov and J. van den Brink, Compass models: Theory and physical motivations, *Rev. Mod. Phys.* **87**, 1 (2015).
- [18] W. M. H. Natori, H.-K. Jin, and J. Knolle, Quantum liquids of the $S = 3/2$ Kitaev honeycomb and related Kugel-Khomskii models, *Phys. Rev. B* **108**, 075111 (2023).
- [19] S. Khatua, M. J. P. Gingras, and J. G. Rau, Pseudo-Goldstone modes and dynamical gap generation from order by thermal disorder, *Phys. Rev. Lett.* **130**, 266702 (2023).
- [20] A. Kitaev, Anyons in an exactly solved model and beyond, *Ann. Phys. (NY)* **321**, 2 (2006).
- [21] G. Jackeli and G. Khaliullin, Mott insulators in the strong spin-orbit coupling limit: From Heisenberg to a quantum compass and Kitaev models, *Phys. Rev. Lett.* **102**, 017205 (2009).
- [22] K. W. Plumb, J. P. Clancy, L. J. Sandilands, V. V. Shankar, Y. F. Hu, K. S. Burch, H.-Y. Kee, and Y.-J. Kim, α - RuCl_3 : A spin-orbit assisted Mott insulator on a honeycomb lattice, *Phys. Rev. B* **90**, 041112(R) (2014).
- [23] A. Banerjee, C. A. Bridges, J.-Q. Yan, A. A. Aczel, L. Li, M. B. Stone, G. E. Granroth, M. D. Lumsden, Y. Yiu, J. Knolle, S. Bhattacharjee, D. L. Kovrizhin, R. Moessner, D. A. Tennant, D. G. Mandrus, and S. E. Nagler, Proximate Kitaev quantum spin liquid behavior in a honeycomb magnet, *Nat. Mater.* **15**, 733 (2016).
- [24] A. Banerjee, P. Lampen-Kelley, J. Knolle, C. Balz, A. A. Aczel, B. Winn, Y. Liu, D. Pajerowski, J. Yan, C. A. Bridges, A. T. Savici, B. C. Chakoumakos, M. D. Lumsden, D. A. Tennant, R. Moessner, D. G. Mandrus, and S. E. Nagler, Excitations in the field-induced quantum spin liquid state of α - RuCl_3 , *npj Quantum Mater.* **3**, 8 (2018).
- [25] J. G. Rau, E. K.-H. Lee, and H.-Y. Kee, Spin-orbit physics giving rise to novel phases in correlated systems: Iridates and related materials, *Annu. Rev. Condens. Matter Phys.* **7**, 195 (2016).
- [26] S. M. Winter, A. A. Tsirlin, M. Daghofer, J. van den Brink, Y. Singh, P. Gegenwart, and R. Valentí, Models and materials for generalized Kitaev magnetism, *J. Phys.: Condens. Matter* **29**, 493002 (2017).
- [27] M. Hermanns, I. Kimchi, and J. Knolle, Physics of the Kitaev model: Fractionalization, dynamic correlations, and material connections, *Annu. Rev. Condens. Matter Phys.* **9**, 17 (2018).
- [28] H. Takagi, T. Takayama, G. Jackeli, G. Khaliullin, and S. E. Nagler, Concept and realization of Kitaev quantum spin liquids, *Nat. Rev. Phys.* **1**, 264 (2019).

- [29] S. Trebst and C. Hickey, Kitaev materials, *Phys. Rep.* **950**, 1 (2022).
- [30] I. Rousochatzakis, N. B. Perkins, Q. Luo, and H.-Y. Kee, Beyond Kitaev physics in strong spin-orbit coupled magnets, *Rep. Prog. Phys.* **87**, 026502 (2024).
- [31] Z. Zhu, I. Kimchi, D. N. Sheng, and L. Fu, Robust non-Abelian spin liquid and a possible intermediate phase in the antiferromagnetic Kitaev model with magnetic field, *Phys. Rev. B* **97**, 241110(R) (2018).
- [32] J. Nasu, Y. Kato, Y. Kamiya, and Y. Motome, Successive Majorana topological transitions driven by a magnetic field in the Kitaev model, *Phys. Rev. B* **98**, 060416(R) (2018).
- [33] S. Liang, M.-H. Jiang, W. Chen, J.-X. Li, and Q.-H. Wang, Intermediate gapless phase and topological phase transition of the Kitaev model in a uniform magnetic field, *Phys. Rev. B* **98**, 054433 (2018).
- [34] M. Gohlke, G. Wachtel, Y. Yamaji, F. Pollmann, and Y. B. Kim, Quantum spin liquid signatures in Kitaev-like frustrated magnets, *Phys. Rev. B* **97**, 075126 (2018).
- [35] H.-C. Jiang, C.-Y. Wang, B. Huang, and Y.-M. Lu, Field induced quantum spin liquid with spinon Fermi surfaces in the Kitaev model, [arXiv:1809.08247](https://arxiv.org/abs/1809.08247).
- [36] C. Hickey and S. Trebst, Emergence of a field-driven U(1) spin liquid in the Kitaev honeycomb model, *Nat. Commun.* **10**, 530 (2019).
- [37] N. D. Patel and N. Trivedi, Magnetic field-induced intermediate quantum spin liquid with a spinon Fermi surface, *Proc. Natl. Acad. Sci. USA* **116**, 12199 (2019).
- [38] L. Zou and Y.-C. He, Field-induced QCD₃-Chern-Simons quantum criticalities in Kitaev materials, *Phys. Rev. Res.* **2**, 013072 (2020).
- [39] J. S. Gordon, A. Catuneanu, E. S. Sørensen, and H.-Y. Kee, Theory of the field-revealed Kitaev spin liquid, *Nat. Commun.* **10**, 2470 (2019).
- [40] D. A. S. Kaib, S. M. Winter, and R. Valentí, Kitaev honeycomb models in magnetic fields: Dynamical response and dual models, *Phys. Rev. B* **100**, 144445 (2019).
- [41] H.-Y. Lee, R. Kaneko, L. E. Chern, T. Okubo, Y. Yamaji, N. Kawashima, and Y. B. Kim, Magnetic field induced quantum phases in a tensor network study of Kitaev magnets, *Nat. Commun.* **11**, 1639 (2020).
- [42] H. Li, H.-K. Zhang, J. Wang, H.-Q. Wu, Y. Gao, D.-W. Qu, Z.-X. Liu, S.-S. Gong, and W. Li, Identification of magnetic interactions and high-field quantum spin liquid in α -RuCl₃, *Nat. Commun.* **12**, 4007 (2021).
- [43] S.-S. Zhang, G. B. Halász, and C. D. Batista, Theory of the Kitaev model in a [111] magnetic field, *Nat. Commun.* **13**, 399 (2022).
- [44] K. Hwang, A. Go, J. H. Seong, T. Shibauchi, and E.-G. Moon, Identification of a Kitaev quantum spin liquid by magnetic field angle dependence, *Nat. Commun.* **13**, 323 (2022).
- [45] S. Feng, A. Agarwala, S. Bhattacharjee, and N. Trivedi, Anyon dynamics in field-driven phases of the anisotropic Kitaev model, *Phys. Rev. B* **108**, 035149 (2023).
- [46] X.-G. Zhou, H. Li, Y. H. Matsuda, A. Matsuo, W. Li, N. Kurita, K. Kindo, and H. Tanaka, Possible intermediate quantum spin liquid phase in α -RuCl₃ under high magnetic fields up to 100 T, *Nat. Commun.* **14**, 5613 (2023).
- [47] Y. Kasahara, T. Ohnishi, Y. Mizukami, O. Tanaka, S. Ma, K. Sugii, N. Kurita, H. Tanaka, J. Nasu, Y. Motome, T. Shibauchi, and Y. Matsuda, Majorana quantization and half-integer thermal quantum Hall effect in a Kitaev spin liquid, *Nature (London)* **559**, 227 (2018).
- [48] T. Yokoi, S. Ma, Y. Kasahara, S. Kasahara, T. Shibauchi, N. Kurita, H. Tanaka, J. Nasu, Y. Motome, C. Hickey, S. Trebst, and Y. Matsuda, Half-integer quantized anomalous thermal Hall effect in the Kitaev material candidate α -RuCl₃, *Science* **373**, 568 (2021).
- [49] P. Czajka, T. Gao, M. Hirschberger, P. Lampen-Kelley, A. Banerjee, J. Yan, D. G. Mandrus, S. E. Nagler, and N. P. Ong, Oscillations of the thermal conductivity in the spin-liquid state of α -RuCl₃, *Nat. Phys.* **17**, 915 (2021).
- [50] J. A. N. Bruin, R. R. Claus, Y. Matsumoto, N. Kurita, H. Tanaka, and H. Takagi, Robustness of the thermal Hall effect close to half-quantization in α -RuCl₃, *Nat. Phys.* **18**, 401 (2022).
- [51] P. Czajka, T. Gao, M. Hirschberger, P. Lampen-Kelley, A. Banerjee, N. Quirk, D. G. Mandrus, S. E. Nagler, and N. P. Ong, Planar thermal Hall effect of topological bosons in the Kitaev magnet α -RuCl₃, *Nat. Mater.* **22**, 36 (2022).
- [52] Z. Nussinov and G. Ortiz, Sufficient symmetry conditions for topological quantum order, *Proc. Natl. Acad. Sci. USA* **106**, 16944 (2009).
- [53] C. Xu and J. E. Moore, Strong-weak coupling self-duality in the two-dimensional quantum phase transition of $p + ip$ superconducting arrays, *Phys. Rev. Lett.* **93**, 047003 (2004).
- [54] A. Y. Kitaev, Fault-tolerant quantum computation by anyons, *Ann. Phys. (NY)* **303**, 2 (2003).
- [55] J. Vidal, R. Thomale, K. P. Schmidt, and S. Dusuel, Self-duality and bound states of the toric code model in a transverse field, *Phys. Rev. B* **80**, 081104(R) (2009).
- [56] I. S. Tupitsyn, A. Kitaev, N. V. Prokof'ev, and P. C. E. Stamp, Topological multicritical point in the phase diagram of the toric code model and three-dimensional lattice gauge Higgs model, *Phys. Rev. B* **82**, 085114 (2010).
- [57] Y. Kamiya, A. Furusaki, J. C. Y. Teo, and G.-W. Chern, Majorana stripe order on the surface of a three-dimensional topological insulator, *Phys. Rev. B* **98**, 161409(R) (2018).
- [58] V. M. Katukuri, V. Yushankhai, L. Siurakshina, J. van den Brink, L. Hozoi, and I. Rousochatzakis, Mechanism of basal-plane antiferromagnetism in the spin-orbit driven iridate Ba₂IrO₄, *Phys. Rev. X* **4**, 021051 (2014).
- [59] L. Zhang, F. Wang, and D.-H. Lee, Compass impurity model of Tb substitution in Sr₂IrO₄, *Phys. Rev. B* **94**, 161118(R) (2016).
- [60] J. Bertinshaw, Y. Kim, G. Khaliullin, and B. Kim, Square lattice iridates, *Annu. Rev. Condens. Matter Phys.* **10**, 315 (2019).
- [61] E. S. Sørensen, J. Gordon, J. Riddell, T. Wang, and H.-Y. Kee, Field-induced chiral soliton phase in the Kitaev spin chain, *Phys. Rev. Res.* **5**, L012027 (2023).
- [62] E. S. Sørensen, J. Riddell, and H.-Y. Kee, Islands of chiral solitons in integer-spin Kitaev chains, *Phys. Rev. Res.* **5**, 013210 (2023).
- [63] E. Lieb, T. Schultz, and D. Mattis, Two soluble models of an antiferromagnetic chain, *Ann. Phys. (NY)* **16**, 407 (1961).
- [64] I. Affleck and E. H. Lieb, A proof of part of Haldane's conjecture on spin chains, *Lett. Math. Phys.* **12**, 57 (1986).
- [65] M. Oshikawa, M. Yamanaka, and I. Affleck, Magnetization plateaus in spin chains: "Haldane gap" for half-integer spins, *Phys. Rev. Lett.* **78**, 1984 (1997).

- [66] M. Oshikawa, Commensurability, excitation gap, and topology in quantum many-particle systems on a periodic lattice, *Phys. Rev. Lett.* **84**, 1535 (2000).
- [67] J. Jordan, R. Orús, G. Vidal, F. Verstraete, and J. I. Cirac, Classical simulation of infinite-size quantum lattice systems in two spatial dimensions, *Phys. Rev. Lett.* **101**, 250602 (2008).
- [68] R. Orús and G. Vidal, Simulation of two-dimensional quantum systems on an infinite lattice revisited: Corner transfer matrix for tensor contraction, *Phys. Rev. B* **80**, 094403 (2009).
- [69] Y. Motoyama, T. Okubo, K. Yoshimi, S. Morita, T. Kato, and N. Kawashima, TeNeS: Tensor network solver for quantum lattice systems, *Comput. Phys. Commun.* **279**, 108437 (2022).
- [70] See Supplemental Material at <http://link.aps.org/supplemental/10.1103/PhysRevB.109.L241116> for further results and technical details in support of the results presented in the paper.
- [71] S. R. White and R. M. Noack, Real-space quantum renormalization groups, *Phys. Rev. Lett.* **68**, 3487 (1992).
- [72] S. R. White, Density matrix formulation for quantum renormalization groups, *Phys. Rev. Lett.* **69**, 2863 (1992).
- [73] S. R. White, Density-matrix algorithms for quantum renormalization groups, *Phys. Rev. B* **48**, 10345 (1993).
- [74] U. Schollwöck, The density-matrix renormalization group, *Rev. Mod. Phys.* **77**, 259 (2005).
- [75] K. A. Hallberg, New trends in density matrix renormalization, *Adv. Phys.* **55**, 477 (2006).
- [76] U. Schollwöck, The density-matrix renormalization group in the age of matrix product states, *Ann. Phys. (NY)* **326**, 96 (2011).
- [77] I. P. McCulloch, Infinite size density matrix renormalization group, revisited, [arXiv:0804.2509](https://arxiv.org/abs/0804.2509).
- [78] M. Fishman, S. R. White, and E. M. Stoudenmire, The ITensor software library for tensor network calculations, *SciPost Phys. Codebases*, **4** (2022).
- [79] L. C. Venuti and P. Zanardi, Quantum critical scaling of the geometric tensors, *Phys. Rev. Lett.* **99**, 095701 (2007).
- [80] D. Schwandt, F. Alet, and S. Capponi, Quantum Monte Carlo simulations of fidelity at magnetic quantum phase transitions, *Phys. Rev. Lett.* **103**, 170501 (2009).
- [81] A. F. Albuquerque, F. Alet, C. Sire, and S. Capponi, Quantum critical scaling of fidelity susceptibility, *Phys. Rev. B* **81**, 064418 (2010).
- [82] B. Douçot, M. V. Feigel'man, L. B. Ioffe, and A. S. Iosevich, Protected qubits and Chern-Simons theories in Josephson junction arrays, *Phys. Rev. B* **71**, 024505 (2005).
- [83] M. E. Fisher and D. R. Nelson, Spin flop, supersolids, and bicritical and tetracritical points, *Phys. Rev. Lett.* **32**, 1350 (1974).
- [84] T. Devakul, S. A. Parameswaran, and S. L. Sondhi, Correlation function diagnostics for type-I fracton phases, *Phys. Rev. B* **97**, 041110(R) (2018).
- [85] E. S. Sørensen, A. Catuneanu, J. S. Gordon, and H.-Y. Kee, Heart of entanglement: Chiral, nematic, and incommensurate phases in the Kitaev-gamma ladder in a field, *Phys. Rev. X* **11**, 011013 (2021).
- [86] S. Khatua, G. C. Howson, M. J. P. Gingras, and J. G. Rau, Ground state properties of the Heisenberg-compass model on the square lattice, [arXiv:2404.02196](https://arxiv.org/abs/2404.02196).
- [87] <https://sharcnet.ca>.
- [88] <https://alliancecan.ca>.